

Negative turbulent production during flow reversal in a stratified oscillating boundary layer on a sloping bottom

Bishakhdatta Gayen and Sutanu Sarkar

Citation: *Physics of Fluids* (1994-present) **23**, 101703 (2011); doi: 10.1063/1.3651359

View online: <http://dx.doi.org/10.1063/1.3651359>

View Table of Contents: <http://scitation.aip.org/content/aip/journal/pof2/23/10?ver=pdfcov>

Published by the [AIP Publishing](#)

Articles you may be interested in

[Internal wave and boundary current generation by tidal flow over topography](#)

Phys. Fluids **25**, 116601 (2013); 10.1063/1.4826984

[Runup and boundary layers on sloping beaches](#)

Phys. Fluids **25**, 012102 (2013); 10.1063/1.4773327

[Nonlinear Marangoni waves in a two-layer film in the presence of gravity](#)

Phys. Fluids **24**, 032101 (2012); 10.1063/1.3690167

[Turbulent boundary layer flow subject to streamwise oscillation of spanwise wall-velocity](#)

Phys. Fluids **23**, 081703 (2011); 10.1063/1.3626028

[Tidal flow over three-dimensional topography in a stratified fluid](#)

Phys. Fluids **21**, 116601 (2009); 10.1063/1.3253692



Negative turbulent production during flow reversal in a stratified oscillating boundary layer on a sloping bottom

Bishakhdatta Gayen and Sutanu Sarkar^{a)}

University of California San Diego, La Jolla, California 92093, USA

(Received 30 June 2011; accepted 8 September 2011; published online 19 October 2011)

Three-dimensional direct numerical simulations are performed to model an internal tidal beam at near-critical slope, and the phase dependence of turbulent processes is investigated. Convective instability leads to density overturns that originate in the upper flank of the beam and span the beam width of 6 m during flow reversal from downslope to upslope boundary motion. During this flow reversal event, negative turbulent production is observed signaling energy transfer from velocity fluctuations to the mean flow. In this note, we explain the mechanism underlying negative production. © 2011 American Institute of Physics. [doi:10.1063/1.3651359]

Oceanic internal tides occur as a baroclinic internal wave response to the flow of the barotropic tides over topography. Internal tides play a dominant role in deep ocean mixing near submarine ridges,^{1,2} continental slopes,^{3,4} and deep rough topography⁵ resulting in modification of the vertical stratification and large scale ocean circulation. In the vicinity of critical slopes, where the slope angle matches the phase of the internal waves, there is resonance and enhanced turbulence is possible as part of the nonlinear response. Aucan *et al.*¹ observed tidally driven overturns with vertical scales of order 100 m at Kaena Ridge. Peak near-bottom dissipation rate of 2×10^{-6} W/kg was observed at that bottom mooring with the corresponding time-averaged value of 1.2×10^{-8} W/kg (10-100 times the ocean interior value), as part of the Hawaii Ocean Mixing Experiment (HOME). Similarly, Nash *et al.*⁴ reported two deep ocean hotspots of turbulent mixing, both at near-critical regions of the Oregon continental slope. Therefore, there is much current interest in understanding bottom turbulence processes associated with internal tides at sloping topography.

Internal tides in critical environments form internal tidal beams resulting in intensified oscillating boundary flow along the slope.^{6,7} Laboratory⁸ and numerical^{6,9} experiments have shown evidence of turbulence in tidal beams over slope topography with length of the order $\mathcal{O}(1-30)$ m and width up to 0.2 m. Recently, Gayen and Sarkar¹⁰ scaled up the generation problem to a beam of width 60 m and a peak velocity of 0.125 m/s using large eddy simulation (LES). Phase-dependent turbulence characteristics, similar to the observations of Aucan *et al.*¹ at Kaena Ridge, were found including turbulence spanning the beam during flow reversal from downslope to upslope. Here, we report on direct numerical simulations (DNS) of the problem of an internal wave beam with a reduced width of 6 m that, while larger compared to the beam width in our previous inhomogeneous studies^{6,9} so that the near-wall turbulence is separated from the beam core, is small enough to permit the DNS approach. All terms in the transport equation of turbulent kinetic energy are computed without recourse to turbulence models.

Oscillating flow over sloping topography with regions of critical slope angle was numerically modeled in our earlier studies^{6,9} using a boundary-conforming grid, curvilinear coordinates, and allowing for streamwise inhomogeneity. Intensified boundary flow creates a baroclinic response in the form of an internal wave beam leading to turbulence. In the present work, we have scaled up the beam width, l_b , and peak near-bottom velocity, U_b , on a slope and investigated phase-dependent turbulence activity in a small segment of the beam.

DNS is used to obtain the velocity and density fields by numerical solution of the Navier-Stokes (NS) equations under the Boussinesq approximation, written in rotated coordinates $[x_r, y_r, z_r]$ in dimensional form as

$$\begin{aligned} \nabla_r \cdot \mathbf{u}_r &= 0 \\ \frac{D\mathbf{u}_r}{D_r t} &= -\frac{1}{\rho_0} \nabla_r p^* + \nu \nabla_r^2 \mathbf{u}_r - \frac{g\rho^*}{\rho_0} [\sin \beta \mathbf{i} + \cos \beta \mathbf{k}] \\ \frac{D\rho^*}{D_r t} &= \kappa \nabla_r^2 \rho^* - (u_r \sin \beta + w_r \cos \beta) \frac{d\rho^b}{dz} \end{aligned} \quad (1)$$

Here, p^* and ρ^* denote deviation from the background pressure and density, respectively. The NS equations are numerically solved to obtain the velocity in rotated coordinates $[u_r, v_r, w_r]$. Numerical methods are discussed in our earlier studies.^{10,11} The test domain, excluding the sponge region, consists of a rectangular box of 5 m length, 16 m height, and 1 m width whose bottom boundary is coincident with the slope topography as shown in Figure 1. The grid size in the test domain is $256 \times 500 \times 128$ in the x_r , z_r , and y_r directions, respectively, with stretching in the z_r direction. The grid spacing ($\Delta x_r = 0.01953$ m, $\Delta y_r = 0.0078$ m, $\Delta z_{r,min} = 0.0021$ m, $\Delta z_{r,max} = 0.2$ m) provides sufficient resolution: $\Delta x_r^+ < 15$, $\Delta y_r^+ < 10$, and $\Delta z_{r,min}^+ < 2$ in terms of the viscous wall unit ν/u_τ . Here, u_τ is the friction velocity defined as $u_\tau = \sqrt{\nu[(\partial \langle u_r \rangle / \partial z_r)^2 + (\partial \langle v_r \rangle / \partial z_r)^2]_{z_r=0}^{1/4}}$. The grid spacing through the domain and at all times satisfies $\Delta z/\eta < 3$ so that the elevated dissipation during convective overturns is also resolved. Periodicity is imposed in the spanwise, y_r , and streamwise, x_r , directions. Zero velocity and a zero value for wall-normal total density flux, i.e., $d\rho/dz_r = 0$ are imposed at

^{a)}Electronic mail: sarkar@ucsd.edu.

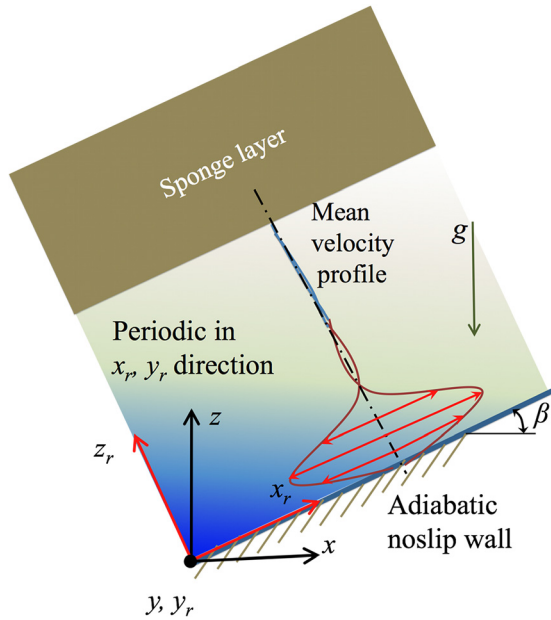


FIG. 1. (Color online) Schematic of the problem. Background shades in the figure indicate the stable density stratification.

the bottom. The sponge region, with damping to the background state, contains 13 points, extends from 16 m to 20 m, and has a maximum $\Delta z_r = 0.49$ m. The upper boundary of the sponge region is an artificial boundary where Rayleigh damping or a “sponge” layer is used. A detailed description motivating the modeling of the tidal beam in a homogeneous domain is available in previous work by Gayen and Sarkar.¹⁰

In the present simulation, $N_\infty = 1.6 \times 10^{-3} \text{ rad.s}^{-1}$ and $\Omega = 1.4076 \times 10^{-4} \text{ rad.s}^{-1}$ giving a wave angle $\theta = \sin^{-1}(\Omega/N_\infty) \approx 5^\circ$. For slope angle, $\beta = 5^\circ$, the criticality parameter is given by $\epsilon = \tan \beta / \tan \theta \approx 1$. The kinematic viscosity, $\nu = 10^{-6} \text{ m}^2/\text{s}$, is that of water. The Prandtl number is chosen to be $Pr = 7$. The beam velocity amplitude is chosen to be $U_b = 0.0125 \text{ m/s}$, and the beam width is $l_b = 6 \text{ m}$. Cycle-averaged and maximum values of turbulent Reynolds number are $Re_T \sim 1500$ and ~ 6000 , respectively. Here, Re_T is based on the velocity scale, $u_T = (1/l_b) \int_{z_r=0}^{l_b} \sqrt{2K} dz_r$, where $K = 1/2 \langle u_i' u_i' \rangle$ is the turbulent kinetic energy, l_b is length scale, and μ is the molecular viscosity. Another Reynolds number is $Re_S = U_b \delta_s / \nu \sim 1500$ based on the Stokes boundary layer thickness $\delta_s = \sqrt{2\nu/\Omega}$. Variable time stepping with a fixed Courant-Friedrichs-Lewy number 1.2 is used leading to $\Delta t \simeq \mathcal{O}(1)$ s. One tidal cycle takes approximately 1500 CPU hours.

The velocity profile, see schematic of Figure 1, corresponds approximately to an oscillating wall jet in a stratified fluid. The phase variation of turbulence over a single tidal period was discussed in our previous LES¹⁰ and is summarized below for the current DNS. Throughout the tidal cycle, the deviation density ρ^* lags the velocity by approximately $\pi/2$, resulting in the maximum of the density deviation during the phase of minimum velocity and vice-versa. The cycle starts with negative peak velocity corresponding to $\phi = 0$ with little deviation of the density field from the background state. Soon after, during the decelerating phase of the downslope flow spanning $0 < \phi < \pi/2$, the density field changes in

response to warmer fluid moving down from upslope to replace the cold fluid previously inside the jet. It is noted that, away from the jet core, the deformation of the density field decreases especially at the top edge of the beam due to relatively low jet velocity. As a result, a density inversion is observed in the upper flank of the beam. Later in time, the large-scale overturns collapse and break into smaller structures. Similarly, during flow reversal from upslope to downslope flow, a density inversion of heavier fluid over lighter fluid occurs inside the lower flank of the jet spanning $0 < z_r < 1$.

The velocity and the density structures formed during the flow reversal event have strong impact on turbulent statistics, calculated here as averages over $x_r - y_r$ planes parallel to the slope. The turbulent kinetic energy, $K = 1/2 \langle u_i' u_i' \rangle$ also denoted by TKE, represents the energy in fluctuations with respect to the mean velocity and satisfies the following evolution equation:

$$\frac{\partial K}{\partial t} = P - \epsilon + B - \frac{\partial T}{\partial z_r}. \quad (2)$$

Here, $\partial T / \partial z_r$ denotes the transport of the TKE consisting of pressure transport, turbulent transport, and viscous transport. P , ϵ , and B are the production, dissipation, and the buoyancy flux, respectively. Figure 2(a) shows the evolution of turbulent kinetic energy, K . Peak TKE that extends up to a height of ~ 8 m above bottom, occurs during the flow reversal due to the large density inversion in the upper flank of the beam. Figure 2(b) shows the temporal evolution of depth-averaged values of each term in the TKE-budget over a tidal period. The depth-averaged buoyancy flux, $\langle B \rangle$, shows positive values during the flow reversal event that correspond to the large density overturn and associated transfer of energy from potential form to kinetic form. Significant negative production $\langle P \rangle$ occurs just after the flow reversal. The event of negative $\langle P \rangle$ spans $\Delta t \sim 1$ h and signals energy transfer from velocity fluctuations to the mean flow. Soon after peak, $\langle B \rangle$, the dissipation, $\langle \epsilon \rangle$, increases. Production regains its positive values after the beam becomes energetic in the upslope direction. Elevated amounts of TKE production and dissipation are observed due to the wall shear during the upslope flow. $\langle P \rangle$ and $\langle \epsilon \rangle$ are the only dominant terms in the TKE-budget during this phase.

Negative turbulent production is an unusual occurrence in boundary layer turbulence. A primary goal of this note is to obtain an explanation for negative production. The mechanism responsible for the observed negative production is explained with the help of the illustration in Fig. 3 and confirmed with the DNS data in Fig. 4. During the decelerating phase of the downslope motion, the downward flow continues to bring water from above in the form of a jet as previously discussed. This creates a density inversion of heavier fluid on top of lighter fluid at the upper flank of the jet as shown in Fig. 3(a). At this phase, the streamwise velocity is small in magnitude but still in the downslope direction.

Soon after, the corresponding unstable density field forms mushroom shaped plumes similar to the Rayleigh-Taylor type instability problem as shown in Fig. 3(b).

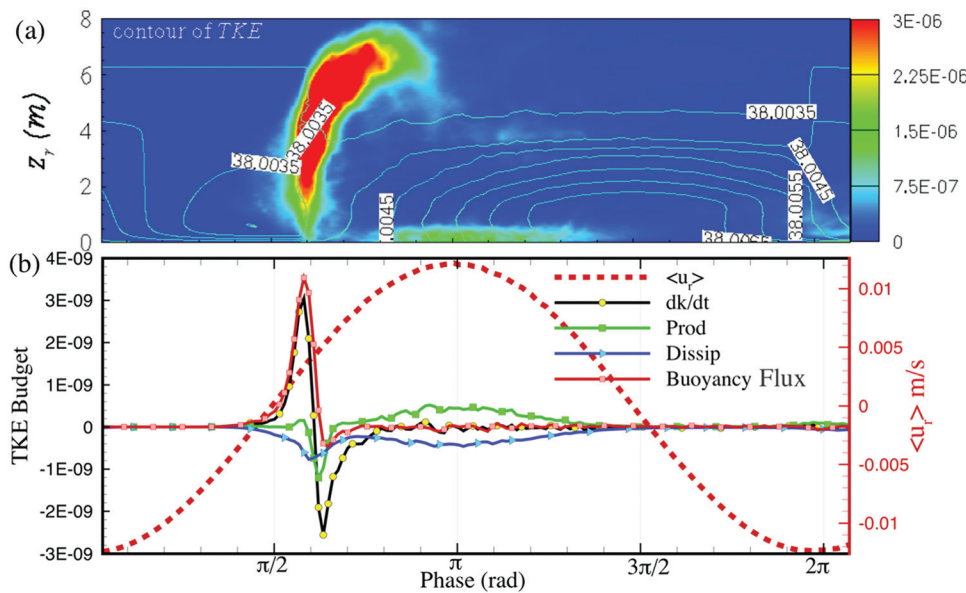


FIG. 2. (Color) (a) Temporal evolution of averaged TKE profiles. (b) Cycle evolution of depth-averaged values of the quantities in TKE-budget along with averaged streamwise velocity (dashed red line) at height of $z^* = 0.6$ m. Here, the averaging region extends from the bottom slope to $z^* = 10$ m.

Structures containing lighter/warmer (heavier/colder) fluid tend to have upward motion, i.e., $w > 0$ (downward motion, i.e., $w < 0$), owing to buoyancy. Thus, velocity fluctuations (mostly up-down vertical motion) are created by positive buoyancy flux during the density inversion, not by background shear associated with the small velocity at this phase.

After the flow reversal, the jet starts to move in the upslope direction with a negative ($d\langle u_r \rangle / dz_r < 0$) velocity gradient in the upper flank of the jet as shown in Fig. 3(c). This sudden applied shear boosts the inclined fluctuating motions of the structures formed before the zero crossing, by providing the rightward streamwise motion for the downward moving structures and vice-versa. This results in negative values of the product of the two velocity components (u'_r, w'_r). The negative Reynolds stress, $\langle u'_r w'_r \rangle$, acts on the negative shear in the upper portion of the jet to give negative turbulent production.

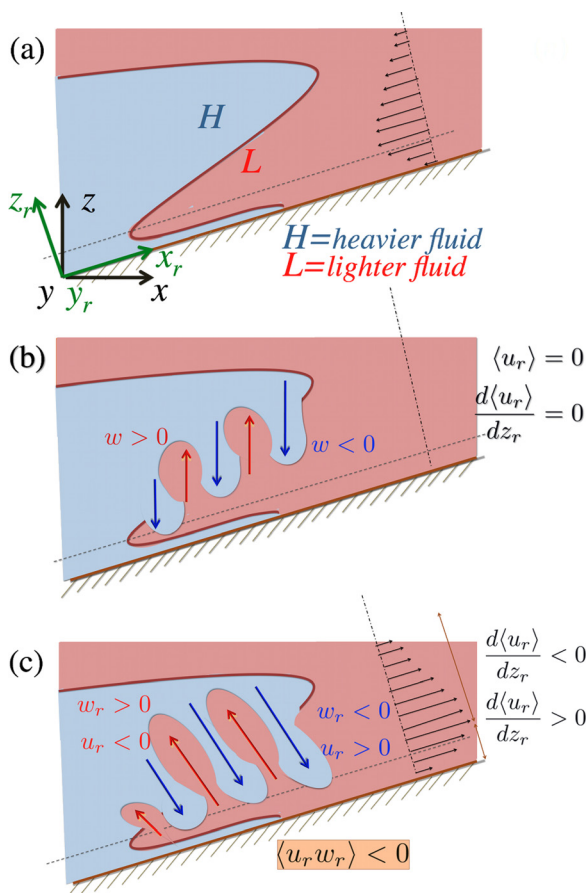


FIG. 3. (Color online) Illustration of negative production mechanism during the flow reversal event from down slope to upslope flow.

To verify this mechanism, snapshots of fluctuating fields are shown in Fig. 4 along with averaged streamwise velocity profile at $\phi = \pi/2 + \pi/10$ at a time immediately after flow reversal from down to upslope motion. Leftward inclined density structures are shown along with their relative motion by the arrows in Fig. 4(b). Figures 4(c) and 4(d) show snaps of the streamwise fluctuating velocity, u'_r and wall normal fluctuating velocity, w'_r , respectively. It is clear that the structures of cold heavier fluid (in blue contour values and white arrows) shown in Fig. 4(b) have positive streamwise velocity in Fig. 4(c) and negative wall normal velocity in Fig. 4(d). Similarly, the lighter fluid structure (in yellow contour values and black arrow) in Fig. 4(b) has negative streamwise and positive wall normal velocity. Consequently, the product of the two components of fluctuating velocity has negative values along the inclined buoyant structures as shown by the white dashed lines in Fig. 4(e) and hence yields a negative value for $P = -\langle u'_r w'_r \rangle \partial \langle u_r \rangle / \partial z_r$ after multiplication with the negative shear in the upper flank of the jet. The duration of negative production is set by the time taken for the convectively driven structures to dissipate.

The interaction of an internal tide beam with a bottom slope has been examined using direct numerical simulation. Immediately after the zero velocity point when the flow reverses from down to upslope, there is a burst of turbulence with large dissipation that spans the beam and lasts for about 1.5 h. This burst is initiated by a convective instability

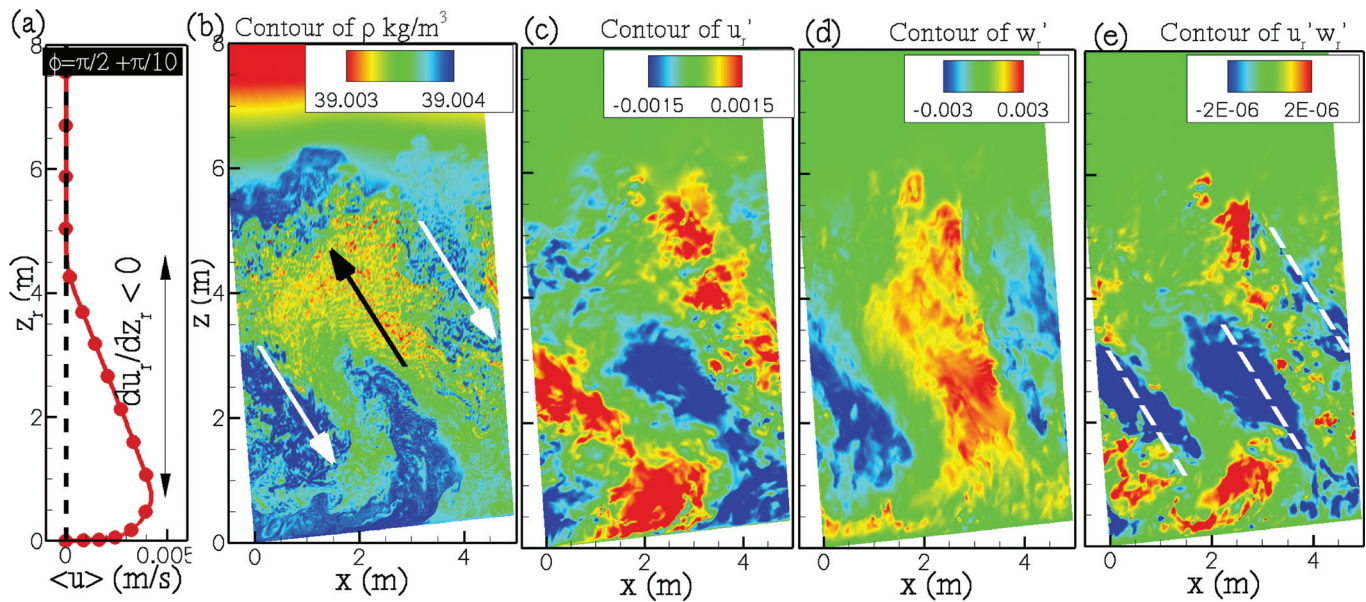


FIG. 4. (Color) (a) Wall normal profiles of mean streamwise velocity at $\phi = \pi/2 + \pi/10$. (a) Vertical x - z slice of the density field (after subtracting 1000 kg m^{-3}) at same phase of (a). Here, back (white) arrow indicates left upward (right downward) motion of the flow structure. Same as (b) for streamwise fluctuation, u'_i (c), wall normal fluctuation, w'_i (c) and their product, $u'_i w'_i$ (e).

detached from the bottom and is accompanied by a large positive buoyancy flux. Negative turbulent production spanning about 1 h occurs during this turbulence episode indicating the transfer of energy from the fluctuating field to the mean field. It is shown that inclined turbulent structures initiated by buoyancy (not shear) are distorted by the non-zero mean shear that occurs after the velocity passes through its zero value, resulting in negative production.

We are pleased to acknowledge support through ONR N000140910287, program manager Terri Paluszkiwicz.

¹J. Aucan, M. A. Merrifield, D. S. Luther, and P. Flament, "Tidal mixing events on the deep flanks of Kaena Ridge, Hawaii," *J. Phys. Oceanogr.* **36**, 1202 (2006).

²D. L. Rudnick and collaborators, "From tides to mixing along the Hawaiian Ridge," *Science* **301**, 355 (2003).

³J. N. Moum, D. R. Caldwell, J. D. Nash, and G. D. Gunderson, "Observations of boundary mixing over the continental slope," *J. Phys. Oceanogr.* **32**, 2113 (2002).

⁴J. D. Nash, M. H. Alford, E. Kunze, K. Martini, and S. Kelly, "Hotspots of deep ocean mixing on the Oregon continental slope," *Geophys. Res. Lett.* **34**, L01605, doi:10.1029/2006GL028170 (2007).

⁵K. L. Polzin, J. M. Toole, J. R. Ledwell, and R. W. Schmitt, "Spatial variability of turbulent mixing in the abyssal ocean," *Science* **276**, 93 (1997).

⁶B. Gayen and S. Sarkar, "Turbulence during the generation of internal tide on a critical slope," *Phys. Rev. Lett.* **104**, 218502 (2010).

⁷H. P. Zhang, B. King, and H. L. Swinney, "Resonant generation of internal waves on a model continental slope," *Phys. Rev. Lett.* **100**, 244504 (2008).

⁸K. Lim, G. N. Ivey, and N. L. Jones, "Experiments on the generation of internal waves over continental shelf topography," *J. Fluid Mech.* **663**, 385 (2010).

⁹B. Gayen and S. Sarkar, "Direct and large eddy simulations of internal tide generation at a near critical slope," *J. Fluid Mech.* **681**, 48 (2011).

¹⁰B. Gayen and S. Sarkar, "Boundary mixing by density overturns in an internal tidal beam," *Geophys. Res. Lett.* **38**, L14608, doi:10.1029/2011GL048135 (2011).

¹¹B. Gayen, S. Sarkar, and J. R. Taylor, "Large eddy simulation of a stratified boundary layer under an oscillatory current," *J. Fluid Mech.* **643**, 233 (2010).